

Self-consistent field theory for obligatory coassembly

I. K. Voets* and F. A. M. Leermakers†

Laboratory of Physical Chemistry and Colloid Science, Wageningen University, Dreijenplein 6, 6703 HB Wageningen, The Netherlands

(Received 11 June 2008; published 8 December 2008)

We present a first-order model for obligatory coassembly of block copolymers via an associative driving force in a nonselective solvent, making use of the classical self-consistent field (SCF) theory. The key idea is to use a generic associative driving force to bring two polymer blocks together into the core of the micelle and to employ one block of the copolymer(s) to provide a classical stopping mechanism for micelle formation. The driving force is generated by assuming a negative value for the relevant short-range Flory-Huggins interaction parameter. Hence, the model may be adopted to study micellization via H bonding, acceptor-donor interactions, and electrostatic interactions. Here, we limit ourselves to systems that resemble experimental ones where the mechanism of coassembly is electrostatic attraction leading to charge compensation. The resulting micelles are termed complex coacervate core micelles (CCCMs). We show that the predictions are qualitatively consistent with a wide variety of experimentally observed phenomena, even though the model does not yet account for the charges explicitly. For example, it successfully mimics the effect of salt on CCCMs. In the absence of salt CCCMs are far more stable than in excess salt, where the driving force for self-assembly is screened. The main limitations of the SCF model are related to the occurrence of soluble complexes, i.e., soluble, charged particles that coexist with the CCCMs.

DOI: [10.1103/PhysRevE.78.061801](https://doi.org/10.1103/PhysRevE.78.061801)

PACS number(s): 36.20.-r

INTRODUCTION

More than 20 years ago a successful model was launched that is able to account for both the starting and the stopping mechanism for self-assembly in a selective solvent, making use of the self-consistent field (SCF) theory. Typical examples that were elaborated on are the formation of micelles by surfactant molecules (ionic as well as nonionic) in water, the formation of bilayer membranes by lipid molecules, again in aqueous solutions, and the formation of polymer micelles via copolymer self-assembly in selective solvents. For such systems, micelles can already form when there are just two components in the system: an amphiphilic entity and a monomeric solvent. The method employs close to molecularly realistic input parameters and allows for semiquantitative predictions of many experimental observables, such as the critical micellization concentration, and structural, mechanical, and thermodynamical quantities, such as density distributions, compressibility, bending moduli, and interfacial tension.

The driving forces for polymer micellization in selective solvents often appear to be extremely strong, leading to kinetically frozen micelles of which the structure invariably depends on the experimental path followed to produce these objects. Although this irreversibility may be beneficial for certain applications where high structural stability is required, here we are interested in micelles that are significantly closer to some thermodynamic control. In the mid-1990s, novel types of polymer micelles that are potential

(near-)equilibrium structures have been developed experimentally [1–3]. They are formed through a coassembly process. Two polymers, of which at least one is a block copolymer, are mixed in a common solvent. One block of the copolymer has a strong affinity to the other chain [1,3], or to one block of the other chain [2]. The polymeric nature gives a cooperativity to the micellization process [1,4], so that the individual contacts, i.e., on the segment level, need not be extremely strong for the associative phase separation to occur. Hence, the driving forces may be relatively weak, leading to potential equilibrium structures with a non-negligible solvent fraction [4,5]. We call this type of assembly (obligatory) coassembly, because the micelle formation occurs only if both molecular species are present in the system. Examples include micelles formed via H bonding, donor-acceptor interactions, and electrostatic interaction. The latter type of micelle is termed a complex coacervate core micelle (CCCMs), after the nature of the driving force, complex coacervation [3]. In the absence of a block (as present in the copolymer) that is not involved in the associative phase segregation process, macroscopic phase separation would have been the result. Indeed, the inactive block accumulates on the outside of the core, providing a classical stopping mechanism and leading to micelles of mesoscopic size. Their exact size and shape is determined by the molecular composition and the strengths of interactions of all molecular species involved.

Since their discovery in 1995 [2], complex coacervate core micelles have been systematically investigated. Their micellization is governed by charge compensation, more precisely by Coulombic attraction and entropy gain through counterion release. At least three chemically different molecules are involved, monomeric solvent and two types of molecules containing charged segments with opposite charge sign. These charged segments often carry annealed charges, which means that the segments do not have a fixed charge,

*Current address: Adolphe Merkle Institute, University of Fribourg, CH-1700 Fribourg, Switzerland.

Email address: ilja.voets@unifr.ch

†frans.leermakers@wur.nl

but there is a certain probability that they may be charged. Their charge density is a function of the solution pH , ionic strength, and proximity to other charged species. Hence, CCCMs are inherently complex species, as their structure and stability depends on a multitude of variables. Apart from those relevant for all micelles stabilized via the classical stopping mechanism—such as core and corona block length, and core to corona block length ratio—several additional factors affecting the strength of electrostatic interactions are of importance, such as the aforementioned charge density and ionic strength. As it is impossible to study all possible scenarios experimentally, and rather difficult and time consuming to investigate all parameters individually (i.e., by varying one parameter while keeping all other parameters fixed), as some are coupled and/or require synthetic efforts, it is fair to say that the field will certainly benefit from a molecular level modeling of these systems.

Recently, there are a few theoretical attempts to model electrostatically driven micellization, where the free energy of micellization explicitly contains a term for the electrostatic driving force [6–9]. Khokhlov *et al.* have considered stoichiometric complexes of ionic-neutral block copolymers and oppositely charged polyelectrolytes [7,8], while Castelnovo has also considered nonstoichiometric conditions [6]. Details of the phase diagram of complex coacervates were predicted more recently by field-theoretical simulations [9]. The corresponding SCF models, which more explicitly account for chain conformations, density profiles, etc., are not yet available, as it is extremely challenging to incorporate all relevant interactions (such as ion correlations on top of the Poisson-Boltzmann equation). Here, we will present a primitive first-order model that captures or mimics the basic features of coassembled systems. It is based on a simplified physical picture, implying that, for example, the chemistry of the charged groups, the electrostatic nature of the driving force, and the local correlation effects between complexed segments are not (explicitly) accounted for. Instead, the key idea is to use a generic associative driving force, generated in a purely pragmatic fashion, to bring two polymer blocks together into the core of the micelle and to employ one block of the copolymer to provide a classical stopping mechanism for micelle formation. This driving force is generated by assuming a negative value for the relevant short-range Flory-Huggins interaction parameter χ . As we will see, such a crude approach is surprisingly capable of mimicking several important physicochemical properties of these systems. For example, to optimize the number of favorable contacts the system automatically tends to evolve toward a state wherein the core has close to equal composition of the attractive species. The theory focuses on the properties of the micelles, while the bulk solution (dilute in polymers) is assumed to be ideal. The latter is known to be an approximation, because even in dilute solutions polymers of opposite charge may form soluble complexes. As a result, we may anticipate artifacts of the SCF model.

It is of interest to mention again that the negative Flory-Huggins parameter imitates the ion correlation problem mentioned above. Indeed, without such correlations the SCF theory is unable to model the assembly of oppositely charged species. The reason is that the complex that is formed is

overall electroneutral and the mean-field electrostatic potential vanishes. As the reference chains in the bulk do not experience an electrostatic potential either (the chains in the bulk remain Gaussian) as well, there is no driving force for the bulk chains to assemble. To go beyond this primitive approach one should do, e.g., field-theoretical simulations along the lines of Lee *et al.* [9], or molecular simulations such as molecular dynamics (MD). Indeed the present ansatz is computationally the least expensive (by far).

First, we will briefly outline general CCCM characteristics that may be used to check the applicability of the SCF model and subsequently that we might gain a deeper understanding of via the modeling. Then, the SCF model and underlying theory is discussed. Consecutively, we will present results on the coassembly of two homopolymers in a nonselective solvent, giving rise to a macroscopic associative phase separation. This study provides us with relevant parameters that will be used in the subsequent section on the coassembly of diblock copolymers giving rise to the formation of mixed micelles. Finally, micellization in asymmetric ternary systems will be addressed briefly, i.e., the coassembly of a diblock copolymer and a homopolymer.

CCCM characteristics

One of the most fundamental characteristics of complex coacervate core micelles is their tendency toward local charge compensation. Indeed, the driving force for micellization is electrostatic in nature, but upon complexation the mean electrostatic potential vanishes. It is necessarily replaced by local electrostatic forces driving positive segments to be near negative segments, thereby holding the micelles together. Hence, in the micellar core, the number of positive and negative charges is approximately equal, and if there is a disparity between these two types of segments, there is monomeric salt that will prevent the build-up of huge electrostatic potentials [4,5]. This brings us to another generic feature, the destabilization of CCCMs upon addition of an excess of monomeric salt via charge screening. Above a certain ionic strength, denoted as the critical ionic strength, micelles can no longer be observed experimentally [1,3,4]. Other general physicochemical properties are rather high critical micellization concentrations (CMCs), polydispersities (in size), and solvent fractions, as compared to other types of polymer micelles, and rather low aggregation numbers. It seems likely that these differences are related to the relative weak nature of the driving force, i.e., electrostatic interaction, as compared to hydrophobic interaction. Similarly, it may render (some) CCCMs near-equilibrium structures.

THEORY

Thermodynamics

The thermodynamic analysis of micelle formation is generic. Hence, the type of driving force, i.e., whether it is associative (giving rise to obligatory coassembly) or segregative (resulting in self-assembly), is immaterial for a macroscopic description. Therefore, we can make use of the ex-

isting thermodynamic framework and extend it to the present system. According to thermodynamics of small systems [10–12], the central quantity of interest is the (excess) grand potential ε of a micelle, which may also be interpreted as the work of formation of the micelle.

In a closed system, i.e., an $(\{n_i\}, V, T)$ ensemble, the free energy (Helmholtz energy F) is the characteristic thermodynamic function, with

$$F \equiv U - TS, \quad (1)$$

$$dU = TdS - pdV + \sum_i \mu_i dn_i + \varepsilon dN, \quad (2)$$

so that

$$dF = dU - TdS - SdT = -pdV + \sum_i \mu_i dn_i + \varepsilon dN - SdT, \quad (3)$$

where i is the index referring to the type of molecule, n is the number of molecules, and μ is the chemical potential. The optimization of F to the number of micelles N at constant V , n_i , and T , gives

$$\frac{\partial F}{\partial N} = \varepsilon = 0, \quad (4)$$

i.e., there should be no energy involved in the formation of micelles in accordance with the thermodynamics of small systems. The system is thermodynamically stable when the second derivative of F with respect to N is positive, i.e., F is in a minimum.

Below we will implement a SCF theory that makes use of lattice approximations. In such an approach, a liquid phase is typically considered to be incompressible, meaning that all lattice sites in the system are filled by solvent or segments of molecules. This convention will be followed, i.e., we consider systems that do not have the possibility to change their volume. Hence, the volume work term $-pdV$ [Eq. (2)] can be dropped in the thermodynamic analysis, and by integration over the extensive variables in Eq. (2) the total grand potential reduces to

$$\varepsilon N = F - \sum_i n_i \mu_i. \quad (5)$$

Within the SCF model one can model only one micelle ($N=1$) that sits with its center of mass in the center of the coordinate system, i.e., one typically considers a micelle without translational degrees of freedom. The grand potential in these calculations is identified by ε_m , often referred to as the translationally restricted grand potential:

$$\varepsilon_m = \varepsilon - k_B T \ln \varphi_m, \quad (6)$$

where $-k_B T \ln \varphi_m = -TS_{tr}$, with S_{tr} being the entropy associated with the translational degrees of freedom of the micelle (dilute solutions, no interactions), and ε_m being the intrinsic work of formation of the micelle. Equation (6) can be used to estimate the volume fraction of micelles for a particular case with given $\varepsilon_m > 0$.

Molecular modeling

The lattice and the molecules

Here we follow the method of Scheutjens and Fler, known as the SF-SCF theory. In analogy to the Flory-Huggins theory for polymer solutions, these authors suggested representing a polymer chain by a sequence of segments. As each segment has a length b and all further spatial features of the segments are ignored, the segments are essentially spheres.

The system consists of the following molecules: two polymeric species $A_{N_A} B_{N_B}$ ($i=1$), and $C_{N_C} B_{N_B}$ ($i=2$), monomeric solvent molecules W_1 ($i=3$), and (in some of the calculations) an extra pair of monomers N_1 ($i=4$) and P_1 ($i=5$). Here the subscript indicates the number of repeats of each monomer type. Thus the total number of monomers is given by the set $\{A, B, C, W, N, P\}$. In the following, this set will be referred to by the subscripts A and/or B . For each molecule all segments obtain a ranking number, e.g., for the $i=1$ polymer $s=1, 2, \dots, N_A+N_B$, where the first N_A segments are of segment type A and the remainder is of type B . We introduce chain architecture operators $\delta_{i,s}^A$, which assume the value unity when segment s of molecule i is of segment type A and zero otherwise. For example, $\delta_{2,1}^C=1$ and $\delta_{1, N_A+1}^B=1$, but $\delta_{3,1}^W=0$, because $\delta_{3,1}^W=1$. Note that for $N_B=0$ the system reduces to two homopolymers. Alternatively, we may choose only to remove the B block of the second copolymer, which results in a system with a copolymer, a homopolymer, and a monomeric solvent.

Again following Scheutjens and Fler, and as in the Flory-Huggins theory, the space is subdivided into lattice sites. The characteristic length of a lattice unit is taken identical to the segment size b , such that all segments fit exactly onto the lattice. In the Flory-Huggins theory all lattice sites are identical and there are no spatial gradients in the system. In the Scheutjens-Fler method, however, the lattice sites are arranged in layers, and the mean-field averaging is performed only along lattice sites within such layer. Volume fraction gradients are allowed to develop between layers only. In the classical SF-SCF theory, the lattice layers are parallel arrangements of a very large number of lattice sites L and the flat layers are numbered $z=1, 2, \dots, M$. Below we will use this approach to evaluate the macroscopic phase behavior of polymer mixtures in a nonselective solvent. In the following we will focus on the case of spherical micelles and trust that the applications of the theory for the macroscopic phase behavior will be evident.

To model (spherical) micelles, one should use a spherical coordinate system that consists of shells of lattice sites and use an index r to refer to these layers, $r=1, 2, \dots, M$. The implementation of the spherical coordinate system has been described in the literature several times [13–15]. In short, it follows that the number of lattice sites L in layer r from the center, obeys $L(r) = \frac{4}{3} \pi [r^3 - (r-1)^3]$. Next, there exist transition probabilities $\lambda(r, r')$ to go from a site in layer r to a site in r' by taking a step of length b . In such cases it is clear that one can only end up within the layer, that is, $r=r'$, or in a neighboring layer, $|r-r'|=1$, and thus that $\sum_{r'=r-1, r, r+1} \lambda(r, r') = 1$. These *a priori* transition probabilities

are used to evaluate the short-range lateral interactions between segments as well as in the evaluation of the statistical weights of the chain conformations (both issues will be discussed below).

Polymer chains can exist in many different conformations. Here a conformation is specified by the set of lattice sites in which the segments are positioned. So conformation c of molecule i is given by $c_i = \{(1_i, r_1^c), (2_i, r_2^c), \dots, (s_i, r_s^c)\}$. As the statistical weight of any conformation cannot depend on whether this is evaluated starting from the $s_i=1$ or the $s_i=N_i$ end of the polymer chain, there exists an internal balance equation that links the r dependences of the transition probabilities to the r dependence of the number of lattice sites:

$$L(r)\lambda(r, r') = L(r')\lambda(r', r). \quad (7)$$

The total number of distinguishable conformations of a typical polymer molecule i is very large but can effectively and efficiently be accounted for in a freely-jointed-chain model.

SCF machinery

At the basis of the molecular modeling is the partition function Q , which essentially is the number of relevant distinguishable states that the system can be in. As this partition function is of the mean-field type, there are major approximations involved. For example, the lattice approximations and the fact that the statistical weights of the chains are evaluated using a freely-jointed-chain approximation, as mentioned above. Even more importantly, in a mean-field theory the binary interactions that act between molecules are replaced by the interaction of a molecule with preaveraged surroundings (i.e., the “mean field”). These surroundings may be seen as some external potential field $u(r)$. As these potentials are iteratively adjusted according to the computed surroundings, the optimized potentials are “self-consistent.”

Conjugated to the potentials there are the concentration distributions of the components. In a lattice model typically dimensionless concentrations, i.e., volume fractions φ , are used. These volume fractions φ follow uniquely from the potentials, and as the potentials are functions of the volume fractions, one may also refer to the volume fractions as being self-consistent. In short, it turns out that the free energy, and thus also the grand potential, can be written as functions of the couple $(\varphi_A(r), u_A(r))$. Here the index A refers to the type of segment and r refers to a relevant spatial coordinate. Thus, the machinery of the SCF theory may be schematically summarized by

$$\varphi[u] \Rightarrow u[\varphi], \quad (8)$$

showing that the volume fractions are unique functions of the potentials (left-hand side) and the potentials are unique functions of the volume fractions (right-hand side). (Note that both quantities have an A and r dependence that is not indicated.)

From potentials to volume fractions

At this point we assume that for all coordinates r and for all segment types A the segment potentials are known and

illustrate how one then can compute the volume fraction profiles, that is the volume fraction φ for each coordinate r for each segment type A . When these segment potentials are known it is possible to select the potential experienced by segment s of molecule i at coordinate r by scanning all segment potentials and using the chain architecture operators

$$u_i(r, s) = \sum_A u_A(r) \delta_{i,s}^A. \quad (9)$$

It is well known that there is a strong analogy between the path followed by a diffusing particle and the conformation of a long polymer chain. For a Gaussian chain the analogy is complete because in the Gaussian chain model excluded-volume effects are not accounted for. One can account for the excluded volume of the chains in an approximate way using the Edwards diffusion equation, i.e., diffusion in a potential field $u(r)$:

$$\frac{\partial G_i(r, s)}{\partial s} = \frac{b^2}{6} \Delta G_i(r, s) - \frac{u_i(r, s)}{k_B T} G_i(r, s), \quad (10)$$

where the Laplace operator $\Delta = \nabla^2$ in the spherical coordinates is given by

$$\Delta = \frac{1}{r^2} \frac{\partial}{\partial r} \left(r^2 \frac{\partial}{\partial r} \right).$$

This differential equation must be complemented with proper initial conditions and boundary conditions. Within the Scheutjens-Fleer formalism this equation is represented by a set of recurrence equations, and this implies a subtle shift from the Gaussian chain to the freely-jointed-chain model. The method starts by introducing Boltzmann weights $G_i(r, s) = \exp[-u_i(r, s)/k_B T]$. The chain connectivity is accounted for by two propagators that are started from opposite ends:

$$G_i(r, s|1) = G_i(r, s) \langle G_i(r, s-1|1) \rangle, \quad (11)$$

$$G_i(r, s|N) = G_i(r, s) \langle G_i(r, s+1|N) \rangle, \quad (12)$$

with initial conditions $G_i(r, 0|1) = G_i(r, N+1|N) = 1$ for all r . In these equations the information in the end-point distribution functions G after the vertical bar reminds us about the segment number (chain end) where the propagators were initiated. Here the angular brackets give a three-layer average weighted by the *a priori* step probabilities,

$$\langle X(r) \rangle = \sum_{r'} \lambda(r, r') X(r') \approx X(r) + \frac{b^2}{6} \Delta X(r). \quad (13)$$

In this equation the site average is illustrated on some function X that depends on r . On the right-hand side of Eq. (13) is the continuum analog of the site fraction.

The volume fraction of segment s of molecule i at coordinate r follows from the so-called composition law which combines the two complementary end-point distribution functions that have been initiated at opposite ends:

$$\varphi_i(r,s) = C_i \frac{G_i(r,s|1)G_i(r,s|N)}{G_i(r,s)}. \quad (14)$$

The division by $G_i(r,s)$ is introduced to account for the fact that the potential field experience by segment s of molecule i at coordinate r is accounted for already in both complementary end-point distributions. The normalization constant C_i may be found straightforwardly. It can be shown that

$$C_i = \frac{\varphi_i^b}{N_i} = \frac{n_i}{G_i(N|1)}, \quad (15)$$

where φ_i^b is the volume fraction of molecule i in the bulk (indicated by the superscript b), and n_i is the number of molecules of type i in the system. This quantity is computed from $n_i = \sum_r \sum_s \varphi_i(r,s)L(r)$. The single chain partition function $G_i(N|1)$ gives the combined statistical weight of all possible and allowed conformations of molecule i in the system and follows from $G_i(N|1) = \sum_r G_i(r,N|1)L(r)$. It can be shown that, because the method obeys inversion symmetry, we have $G_i(N|1) = G_i(1|N)$. From Eq. (15) it is clear that either φ_i^b or n_i must be an input quantity for the calculations. However, because there must be an incompressibility condition in the bulk,

$$\sum_i \varphi_i^b = 1, \quad (16)$$

we can compute the normalization for one of the components (typically this is done for the solvent molecule) from the C values of all the other ones. It is of interest to mention that the above propagator scheme also applies to monomeric species. For these components the procedure reduces to $\varphi_i(r) = C_i G_i(r,1)$.

It is convenient to compute from the volume fractions that depend on the segment ranking number, the corresponding quantities that depend on the segment type. These quantities are found by scanning all segment distributions and adding them together if the segments are of the proper type:

$$\varphi_A(r) = \sum_i \sum_s \varphi_i(r,s) \delta_{i,s}^A. \quad (17)$$

Similarly, one can evaluate the volume fraction of A in the bulk, collected in φ_A^b for all segment types A .

From volume fractions to potentials

In this section we assume that the volume fractions of all segment types are known at all coordinates in the system, including the bulk and show that from this the segment potentials follow. Physically, the segment potential at coordinate r of segment type A , should contain the work needed to bring this segment A from infinite distance (somewhere in the bulk where the reference of the potential is chosen) to the coordinate r .

There exists a recipe to obtain the segment potentials that belong to the corresponding Helmholtz energy of the systems. We will not attempt to derive the potentials. Instead the final result will be presented. Only two contributions will be accounted for:

$$u_A(r) = u'(r) + u_A^{\text{FH}}(r). \quad (18)$$

The first term in Eq. (18) is called the Lagrange field. Its value is chosen such that the system obeys the incompressibility condition

$$\sum_A \varphi_A(r) = 1, \quad (19)$$

which should be obeyed at all coordinates r . Physically it may be interpreted as the work needed to give up an empty lattice site in the bulk and to create one at coordinate r . This empty space is needed to place the segment A . This work is independent of the segment type, as all segments in our model are of equal size. When for some reason there are insufficient segments at some coordinate r' , the value of $u'(r')$ will be decreased such that all segment potentials $u_A(r')$ decrease proportionally. This will have the consequence that more segments are attracted to this coordinate, as anticipated. When some coordinate is overpopulated, the value of $u'(r)$ will be increased with the effect that segments are pushed out.

The second term in Eq. (18) is the term that accounts for the short-range interactions between segments and solvent molecules. Within a lattice approach where all lattice sites are filled (incompressible system), it is possible to use Flory-Huggins (FH) parameters $\chi_{AB} = (Z/2k_B T)(2U_{AB} - U_{AA} - U_{BB})$. In this equation, Z is the lattice coordination number, that is, the number of neighbors of a particular lattice site, which is assumed to be constant throughout the lattice. From this FH parameter we see that, when the energetic contributions that originate from a contact between A and B (given by U_{AB}) are higher than the average contributions between an A - A and a B - B contact, A and B repel each other and $\chi_{AB} > 0$. On the other hand when the interaction of an A - B contact is more favorable than the average of A - A and B - B contacts, then the corresponding $\chi_{AB} < 0$ and the system has the tendency to make A - B contacts. Below we will focus on such attractive conditions to generate associative phase segregation and complex coacervate core micelles. Following the Flory-Huggins theory and in its most primitive form, the short-range interactions can be implemented using the Bragg-Williams approximation. Within the Bragg-Williams approximation the probability of having an A - B contact, for a segment A at coordinate r , is given by the volume fraction of B at this coordinate, and thus

$$u_A^{\text{FH}}(r) = \sum_B \chi_{AB} (\langle \varphi_B(r) \rangle - \varphi_B^b), \quad (20)$$

where the angular brackets implement the fact that an A - B contact can also take place between two segments that are in neighboring lattice layers. The quantity φ_B^b is introduced to normalize the segment potentials to be zero in the bulk. In many SCF approaches the angular brackets in the segment potentials are omitted. Note, however, that these angular brackets are essential especially for systems that feature strong volume fraction gradients.

Numerical solution

The above set of equations is closed and may be solved numerically once proper boundary conditions have been specified. In principle, there are only two coordinates that need special attention, that is, $r=0$ and $r=M+1$. As there are no lattice sites at $r=0$, there is no need to worry about this side of the system. At the other side of the system, however, we have implemented reflecting boundary conditions. This means that, for all relevant quantities $X(r)$, we have implemented $X(M+1)=X(M)$. Such reflecting boundary conditions are needed in the propagators where, e.g., $G_i(M+1, s|1)=G_i(M, s|1)$ for all s values. Also for all volume fraction distributions, we have $\varphi_i(M+1, s)=\varphi_i(M, s)$. Typically, however, the value of the last layer M in the system is chosen to be so large that around $r=M$ the homogeneous bulk is present. In this case the reflecting boundary condition is inconsequential for any system property.

Solutions of the equation have the property of self-consistency. This means that the segment potentials both follow from the volume fractions, and also determine the volume fractions, and conversely the segment volume fractions both follow from the potentials and determine them. In addition, the incompressibility condition is obeyed at all coordinates. Below, the volume fractions and the segment potentials are accurate in at least seven significant digits which are routinely generated using a numerical iterative scheme based upon a quasi-Newton iteration. The high accuracy is needed to accurately determine the thermodynamic properties of the micelles in the system.

Thermodynamic quantities

For a given SCF solution the mean-field partition function is available and from these quantities various observables can be computed. Typically, the number of molecules is fixed (canonical ensemble) and an appropriate thermodynamic analysis is needed to select relevant micelles from the possible sets of generated micelles. The central quantity is the grand potential ε_m , which is computed as $\varepsilon_m=F-\sum_i \mu_i n_i$. It turns out that the grand potential can be written as a function of the potentials and segment volume fractions. The grand potential is built up from a summation over the so-called grand potential density ω , i.e., $\varepsilon_m=\sum_r \omega(r)L(r)$. In turn, the grand potential density is given by

$$\frac{\omega(r)}{k_B T} = - \sum_A \varphi_A(r) \frac{u_A(r)}{k_B T} - \sum_i \frac{\varphi_i(r) - \varphi_i^b}{N_i} + \frac{1}{2} \sum_A \sum_B \chi_{AB} \{ \varphi_A(r) \times [\langle \varphi_B(r) \rangle - \varphi_B^b] - \varphi_A^b [\varphi_B(r) - \varphi_B^b] \}. \quad (21)$$

Below we will further need a measure of the micelle size. There are many ways to characterize the size of the micelle. Here we choose to focus on the average position of the segments B that typically are located in excess in the corona. So for any volume fraction distribution of the B block, $\varphi_B(r)$, and bulk volume fraction of the B segments, φ_B^b , the first moment of R can be computed from

$$R = \frac{\sum_r L(r)r(\varphi_B(r) - \varphi_B^b)}{\sum_r L(r)(\varphi_B(r) - \varphi_B^b)}, \quad (22)$$

where it is understood that R is in units of lattice site length b .

Parameters

One of the complications of modeling obligatory coassembly over classical self-assembly is the large parameter space that characterizes the system. It will prove impossible to consider all relevant cases. The choice of some of the parameters used below stems from available experimental systems. Furthermore, we opted for the simplest systems, wherein the number of different parameters is at a minimum.

Before we consider micelle formation, we first need to identify the relevant values for the two interaction parameters χ and χ_{AC} . A reasonable value of these parameters corresponds to sufficient driving force for the assembly process. We may find out whether or not this is the case by considering the system of two homopolymers A_{N_A} and C_{N_C} (and thus $N_B=0$) in the monomeric solvent W . Of course this system cannot give rise to the formation of stable micelles. Instead, one finds phase coexistence between a phase rich in the polymeric components A and C (phase α) and another phase (phase β) rich in the solvent. The Flory-Huggins free energy density for a phase with densities φ_A , φ_C , and φ_W is given by

$$\frac{f}{k_B T} = \varphi_W \ln \varphi_W + \frac{\varphi_A}{N_A} \ln \varphi_A + \frac{\varphi_C}{N_C} \ln \varphi_C + \chi_{AC} \varphi_A \varphi_C + \chi \varphi_W (\varphi_A + \varphi_C) \quad (23)$$

and can be used to optimize the total free energy of a system,

$$\frac{f^{\text{tot}}}{k_B T} = V^\alpha \frac{f^\alpha}{k_B T} + V^\beta \frac{f^\beta}{k_B T}, \quad (24)$$

under the incompressibility constraint $\varphi_A + \varphi_C + \varphi_W = 1$. As mentioned already, it is also possible to make use of the SCF approach to find the composition of coexisting phases. As a bonus one can then also compute the interfacial profile that develops between the two coexisting phases and evaluate the corresponding interfacial tension. The machinery is straightforwardly adjusted to this problem. First, a flat lattice geometry suffices (for this case the coordinate z is used) and is implemented by inserting λ values that do not depend on the layer number. Second, the boundary condition near $z=1$ is treated similarly as the boundary near layer $z=M$. For the phase coexistence study, $M=500$ lattice sites are taken and throughout this paper, $\lambda=1/3$ is used.

For the micellar case, the minimum number of different molecules is three; one monomeric solvent W and two polymeric species, of which at least one is a copolymer. We restrict ourselves to $N_A=N_C=40$. The length of the corona block N_B will be kept as a variable, but will typically be much larger than the core forming blocks. Fundamental to the obligatory coassembly idea is that the solvent is nonselective, e.g., it is a good or at least a θ solvent for all blocks.

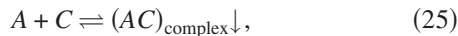
Thus, we are left with a choice of the relevant values for the FH interaction parameters, such as χ_{AC} , the driving force for coassembly, which we base upon the study on the coacervation of A_{N_A} and C_{N_C} described below. As default, $\chi_{AC}=-2$ is chosen, which gives rise to a strong driving force, as we will see in the following section. The set of FH interaction parameters that includes the solvent is $\chi_W \equiv \chi_{AW} = \chi_{BW} = \chi_{CW}$. The interactions of the corona forming block with the core-forming one, $\chi_B \equiv \chi_{AB} = \chi_{BC}$ is the third set of parameters. For simplicity, $\chi \equiv \chi_W = \chi_B$ and $\chi=0.5$ are chosen as the default.

RESULTS

Let us start with the phase behavior of two homopolymers giving rise to associative phase segregation, i.e., complex coacervation. From this study, a default set of parameters is selected that will be applied to the more complicated case of coassembly, i.e., micellization. The molecular structures are chosen to resemble experimental systems. For the same reason we will focus on spherical micelles only. Qualitative consistency with a wide variety of experimentally observed phenomena will be discussed.

Associative phase segregation in a ternary system of two homopolymers in a nonselective solvent

In this section, we will consider systems consisting of two homopolymers ($N_B=0$) that attract each other, dissolved into a nonselective solvent. Thus



where the \downarrow indicates the formation of an $(AC)_{\text{complex}}$ -rich phase. By symmetry (both chains are equally long, i.e., $N_A = N_C = 40$), the stoichiometric ratio of A and C is 1:1 and the $(AC)_{\text{complex}}$ phase forms above some threshold concentration (i.e. the solubility limit). The goal of this section is to identify suitable values of the interaction parameters relevant for the driving forces that give rise to micelle formation in an obligatory coassembly process.

We start by analyzing a set of volume fraction profiles for systems that are in a two-phase state (Fig. 1). In both Figs. 1(a) and 1(b) we present three sets of volume fraction profiles for three values of the strength of the driving force for phase separation, i.e., $\chi_{AC} = -2, -1.5, \text{ and } -1$. In these calculations, the volume of the system was fixed to $M=500$ lattice layers. In all calculations, the amount of both polymers in the system is set, i.e., the total amount of polymer $\theta_A + \theta_C$ is set to 100 equivalent monolayers (1/5 of the system is filled by polymer). In Fig. 1(a) we have equal amounts of the two polymers in the system, whereas in Fig. 1(b) there is three times as much of A as of C. In both graphs we see that the volume fraction profiles are rather simple. The polymer-rich phase (phase α) is homogeneous up to close to the interface, where it drops sharply, until a second homogeneous value in the water-rich phase (phase β) is found. The interface shifts to higher z values when the driving force is reduced, that is, for less negative χ_{AC} . As the amount of polymer is fixed, the amount of water in the polymer-rich phase increases with

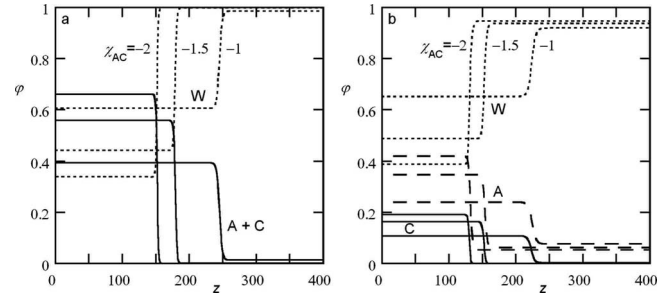


FIG. 1. Three sets of volume fraction profiles across the interface between a polymer-rich phase (phase α ; low z values), and a solvent-rich phase (phase β ; high z values), $N_A = N_C = 40$, $\chi = 0.5$, for three values of the interaction parameter $\chi_{AC} = -2, -1.5, \text{ and } -1$ as indicated. (a) For equal amounts of the two polymers, i.e., $\Theta_A = \Theta_C = 50$. As in this case $\varphi_A(z) = \varphi_C(z)$, the sum of these is presented as the solid lines. The dotted lines are the solvent profiles. (b) For three times as much of polymer A as of polymer C, i.e., $\Theta_A = 75$ and $\Theta_C = 25$. The solvent is dotted, the A segments are dashed, and the C profile is given by the solid lines. Only 400 of the 500 layers that were in the system are plotted.

decreasing strength of the attraction between A and C. In Fig. 1(a) we present the sum of the volume fractions of both polymers (as they are equal in this case). In Fig. 1(b) the compositions of A and B are very different and therefore both profiles are presented separately. The need to optimize the amount of A-C contacts (i.e., the need to maximize $\varphi_A \varphi_C$), results in the polymer-rich phase in a ratio $R^\alpha = \varphi_A(1) / \varphi_C(1) = 2.18, 2.11, \text{ and } 2.22$, i.e., of order unity, for $\chi_{AC} = -2, -1.5, \text{ and } -1$, respectively. In the β phase, however, the ratio is a much stronger function of the attraction, and $R^\beta = \varphi_A(500) / \varphi_C(500) = 2.3 \times 10^6, 3 \times 10^3, \text{ and } 23$ for $\chi_{AC} = -2, -1.5, \text{ and } -1$, respectively. The volume fractions that exist near the system boundaries, that is, near $z=1$ and 500 are the binodal values. Even though the overall amount of polymer in both graphs is identical, the interface is consistently shifted to higher z values when the composition is 1:1 compared to the 3:1 composition. This means that in the symmetric case more of the polymer is collected in the polymer-rich phase and the overall polymer concentration in the solvent-rich phase is lower than in the asymmetric systems.

Figure 2(a) shows typical results for the phase diagrams. All compositions (φ_C, φ_A) within the closed line are unstable and will separate into two phases. Compositions outside this area are stable and the system remains in the one-phase state. The lines in the phase diagram represent the combinations φ_A and φ_C that occur in the system when it actually has separated into two phases. The lines are generated by systematically varying the ratio of the two polymers in the system (the homogeneous system would represent a point inside the lines). As our system is symmetric with respect to the exchange of C with A, the phase diagram is symmetric with respect to the line $\varphi_A = \varphi_C$. The compositions of the concentrated phases (phase α) are given in the top right part of the curve and, in the bottom left, we have the corresponding compositions of the dilute phases. Obviously one point on the top right is connected to a point on the lower part of such

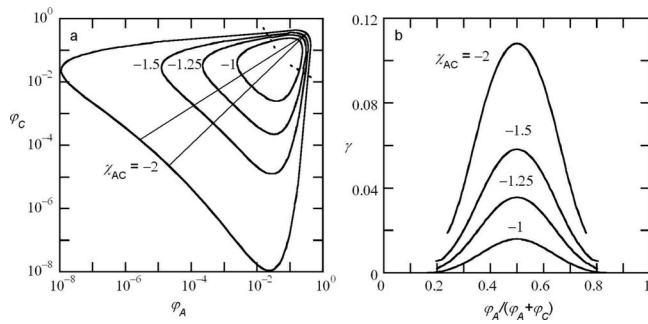


FIG. 2. (a) Phase diagram in the φ_C - φ_A coordinates on a logarithmic scale for four values of the driving force for the phase separation χ_{AC} , as indicated. The dotted line denotes the estimated critical points in these systems. For illustration purposes two tie lines that connect coexisting points are presented as examples. (b) The corresponding interfacial tension (in units of $k_B T$ per unit area b^2) as a function of the fraction of A segments in the polymer-rich phase.

graph. One may present tie lines that connect such coexisting points. For illustrative purposes two of these tie lines are presented in Fig. 2(a). Again the ratio R can vary wildly in the water-rich corner, but it remains much closer to unity in the polymer-rich corner. The dotted line denotes the estimates of the critical points in these systems. At the critical point the composition of the polymer-rich and solvent-rich phases become identical. From the series of phase diagrams it is clear that, when $\chi_{AC} > -1$, the two-phase region will collapse and no phase separation can be found. The exact value of the disappearance of the phase separation will depend on the degree of polymerization as well as χ_{AC} . At this point, we would like to note that the phase diagrams presented in Fig. 2 strongly deviate from the phase diagrams determined experimentally [16,17], as SCF theory does not account for correlations between oppositely charged polymers in bulk, resulting in soluble complexes.

Important for the assembly into micelles is the interfacial tension that develops between the polymer-rich and the solvent-rich phases. The higher the interfacial tension, the smaller the area per polymer, the higher will be the crowding (overlap) of the nonassociating block in the corona. In Fig. 2(b), the interfacial tension in dimensionless units is plotted as a function of the fraction of A polymers in the polymer-rich phase. These curves show that the interfacial tension is at the maximum when the concentration of A and C in the polymer-rich phase is equal and is higher the stronger this attraction is. Indeed in this case the cohesive interactions are at their optimum. The interfacial tension drops upon increasing deviation of the fraction of A in the polymer-rich phase from 0.5. At the same time, the overall polymer concentration in the polymer-rich phase decreases as mentioned above. Upon the approach towards the critical points the interfacial tension drops to zero smoothly. Note that the interfacial tension is significantly lower (by a factor of ten) than for the typical case of segregative phase transitions (we obtain $\sim 0.16 \text{ mN m}^{-1}$ for $\chi_{AC} = -2$, compared to $30\text{--}50 \text{ mN m}^{-1}$ for aliphatic hydrocarbon/water interfaces [18]).

In the above results we focused on the special case that both polymers were in θ conditions, i.e., $\chi = 0.5$. A higher

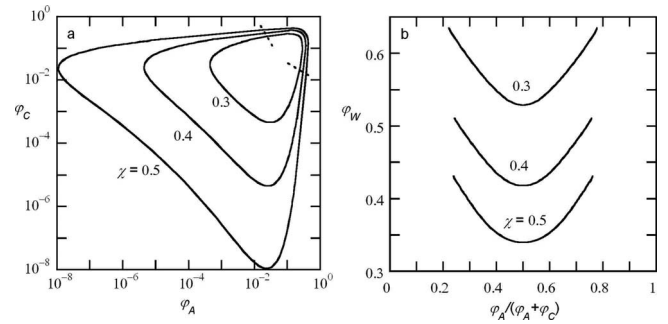


FIG. 3. (a) Phase diagram in the φ_C - φ_A coordinates on a logarithmic scale for three values of the solvent quality χ as indicated for a fixed value of the driving force $\chi_{AC} = -2$. The dotted lines are the estimated critical points in these systems. (b) The corresponding volume fraction of solvent φ_W as a function of the fraction of A segments in the polymer-rich phase.

value corresponds to a poor solvent and will result, for very long polymer chains, in a segregative phase transition. A less positive value, on the other hand, corresponds to good solvent conditions. Polymers in a good solvent have the tendency to accumulate a lot of solvent around their segments. Such hygroscopic effects counteracts the driving force for associative phase transitions. In Fig. 3(a) three phase diagrams are presented for a fixed χ_{AC} for which the solvency is varied from $\chi = 0.5, 0.4$, to 0.3 . As can be seen from this figure, there is a strong effect of the solvent quality. The two-phase region decreases dramatically when the solvent quality is improved. Indeed, most water-soluble polymers have a solubility parameter close to 0.4 and we thus may expect a strong dependency on the type of polymer used in the coassembly process. Note that for the obvious choice, namely, $\chi = 0$, there would not have been a two-phase state, unless one accepts very strong driving forces, i.e., $\chi_{AC} < -2$.

The accompanying Fig. 3(b) provides additional insights into the composition of the polymer-rich phase. For the three phase diagrams presented in Fig. 3(a), the volume fraction of solvent W is shown as a function of the fraction of A chains in the polymer-rich phase. As already anticipated from the volume fraction profiles of Fig. 1, the equal composition A:C is the most favorable, as such a state gives the optimal number of attractive contacts. Above we already showed that this results in a relatively low interfacial tension [Fig. 2(b)] and here we see that it corresponds to a relatively low solvent content. A small improvement of the solvent quality from $\chi = 0.5$ to 0.3 can easily increase the amount of solvent in the polymer-rich phase by a factor of 2. Deviations from the equal composition state also result in a significant uptake of solvent. This can also be as much as a factor of 2. Such effects are important for micelle formation in these systems.

In systems that form polymer-rich phases due to attractive interactions between positively and negatively charged polymers, it is known that the salt concentration can counteract such complexation. Here we show that in the primitive model, where the attractive interactions between plus and minus is represented by an attractive χ parameter, it turns out that it is possible to destroy the formation of a polymer-rich phase by adding monomeric components with similar inter-

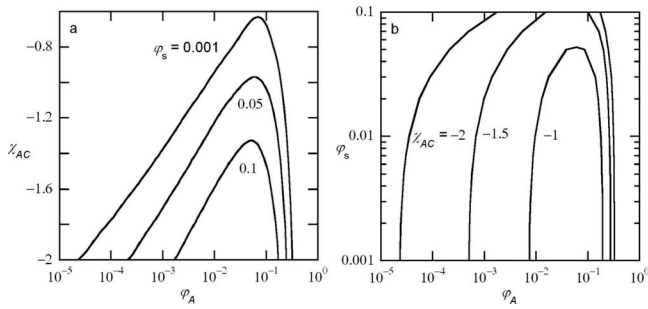


FIG. 4. Phase diagrams for the case that the polymers A and C have equal bulk concentrations (balanced systems) in the presence of a pair of monomers N and P mimicking salt. (a) Binodals with χ_{AC} on the y axis, the concentration of $\varphi_A = \varphi_C$ of the two coexisting phases on the x axis for three values of the salt concentration $\varphi_s \equiv \varphi_N = \varphi_P = 0.1, 0.05$, and 0.001 , as this is present in the phase that is dilute in polymer. (b) Binodals with on the y axis the salt concentration φ_s (in the solvent-rich phase), and the coexisting polymer volume fractions φ_A on the x axis, for three values of the attraction between A and C , χ_{AC} , as indicated. All concentrations are plotted on a logarithmic scale.

actions as the polymers have. So, we introduce a monomeric component N which is energetically equivalent to component A and a monomeric component P which behaves similar as C . To prevent the systems from becoming exceedingly complex, the special case that the two polymers A and C have equal concentrations (both in the dilute as well as in the concentrated phase) is considered. Indeed such a balanced system is expected to give the strongest driving force for the formation of a coacervate phase.

Figure 4 presents a few sets of phase diagrams that illustrate the effect of salt in these systems. In Fig. 4(a) we show for three values of the salt concentration (here defined as the volume fraction of salt in the phase that is dilute in polymer and rich in solvent) the phase diagram in the χ_{AC} - φ_A coordinates. Note that the volume fraction of A is identical to that of C , that is, $\varphi_A = \varphi_C$; similarly, $\varphi_s = \varphi_N = \varphi_P$. Complementary data are shown in Fig. 4(b), where the phase diagram is given in the coordinates φ_s - φ_A for three values of χ_{AC} . From both phase diagrams we conclude that the addition of “salt” screens the complex coacervate phase formation. Even though electrostatic interactions are not explicitly accounted for, we note that the entropic effects that underlie this phenomenon are fully analogous to what happens in true ionic systems. The critical point shifts to a stronger driving force when more salt is added. In other words, there exists, for a given salt concentration, an interaction parameter χ_{AC} below (less negative) which the system remains homogeneous [Fig. 4(a)], or, vice versa, for a given value of the attractive interactions χ_{AC} , there exists a critical salt concentration above which there is no coacervate phase formed. For very strong attractive interactions, the amount of salt needed to remain in the miscible state becomes larger than $\varphi_s = 0.1$. As the polymer concentration near the critical point is also near $\varphi_A = \varphi_C = 0.1$, we tend to go to systems that have gradually less water present. That is why we have not continued the phase diagrams in Fig. 4(b) above $\varphi_s = 0.1$.

Complex coacervate core micelles

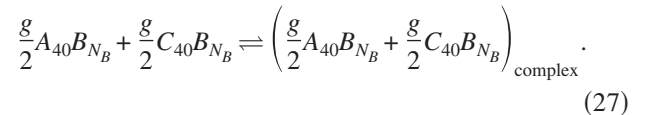
In the previous section we have seen that $\chi_{AC} = -2$ gives a sufficiently strong driving force for association of chains with length $N=40$, and that this association can be destroyed by the addition of monomeric species. We also arrived at the conclusion that for this association the solvent quality is important: it should not be too good. For this reason, $\chi=0.5$ will be used as a default. We now proceed by analyzing the formation of micelles by considering a pair of copolymers $i=1, A_{40}B_{N_B}$, and $i=2, C_{40}B_{N_B}$. The copolymers have an associating block of the same length and identical nonassociating block with the length N_B . Such a system is fully symmetric with respect to the structural composition.

The first set of results will focus on the condition that in the bulk the volume fraction of both copolymers is the same. The resulting micelles will thus have the same number of molecules of both polymers. The aggregation number g is computed by the excess of both molecules in the micelle

$$g = \sum_{i=1,2} \sum_r \frac{L(r)[\varphi_i(r) - \varphi_i^b]}{N_B + 40}. \quad (26)$$

Symmetric ternary systems

We focus on micelle formation that can conveniently be represented by the equilibrium



Let us first give a few typical radial volume fraction profiles for micelles composed of copolymers by way of the obligatory coassembly process. First, we focus on the CMC, which corresponds here to the overall (bulk) volume fraction of polymer above which micelles are present and below which the copolymers remain dissolved as monomeric species. The micelles that exists at the CMC are the smallest possible (have the lowest aggregation number). In Fig. 5(b) the grand potential of stable micelles is plotted as a function of the aggregation number g . In this figure the smallest micelles that are stable are indicated by the open spheres. With increasing corona block length N_B , the first stable micelles have a lower aggregation number g , which is in line with experimental observations [19,20]. In Fig. 5(a) the radial volume fraction profiles are given for $N_B = 50, 100, 200$, and 400 . The volume fraction of the core forming blocks ($A+C$) goes to a fixed volume fraction of $\varphi_{\text{core}} \sim 0.7$ for all micelles, i.e., both φ_W and $\varphi_A = \varphi_C$ are independent of N_B . The interface between core and solvent W is rather sharp (occurs over a few lattice layers). The shorter N_B , the higher the aggregation number (at the CMC) and thus the larger is the core. This is seen as the interface between core and corona shifts to larger r values. The corona block (B) extends into the solvent. It has the characteristic bell-shaped profile. For small N_B the CMC is very low and on this scale the volume fraction is not distinguishable from zero. For the longer B blocks this is no longer the case and clearly the profiles level off to a constant value for $r > 30$.

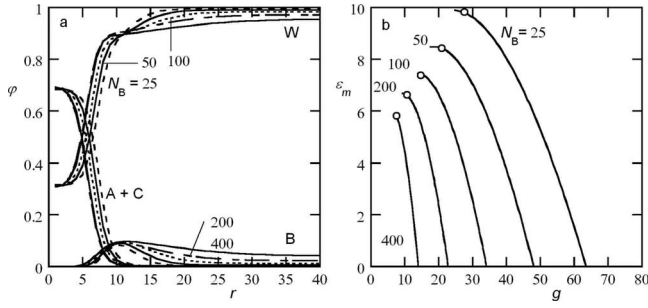


FIG. 5. (a) A set of radial volume fraction profiles for spherical micelles composed of $A_{40}B_{N_B}$ and $C_{40}B_{N_B}$ copolymers, with N_B indicated. The volume fractions of the core blocks A and C are added together (and indicated by $A+C$). The corona block B and the solvent W are plotted separately. All profiles correspond to the first stable micelles (i.e., at the CMC) indicated by the open spheres in (b). (b) The grand potential of the micelle ϵ_m in units of $k_B T$ as a function of the aggregation number g (sum of the excess number of copolymers of both species). Only the relevant part of ϵ_m is plotted, i.e., $\epsilon_m > 0$ and $\partial\epsilon_m/\partial g < 0$. The open spheres point to the smallest stable micelles of which the radial volume fraction profiles are presented in (a) $\chi_{AC} = -2$, $\chi = 0.5$, and $\varphi_1^b = \varphi_2^b$.

By inspection of the graphs of Fig. 5(a), one can easily estimate the size of the core in relation to that of the corona. For all profiles shown, it is true that the size of the corona is larger than that of the core. This indicates that for the present setting the spherical micelles are indeed the stable micellar species [21]. Calculations on cylindrical micelles confirm this (results not shown). Experimentally, spherical CCCMs are widely investigated, whereas other morphologies appear to be far less abundant [2,4,5,19].

We now shift our attention to Fig. 5(b). From the thermodynamics of small systems it follows that with decreasing ϵ_m the translational entropy decreases, which effectively means that the micelle concentration increases. In other words, with increasing micelle concentration the aggregation number increases, until a maximum of about twofold the aggregation number at the CMC. Note that this result applies to homodisperse molecular species. When the copolymers are sufficiently polydisperse (in both core forming as well as corona forming blocks) the opposite trend can be found, i.e., micelles can become smaller upon an increase in micelle concentration [21].

As mentioned above, a characteristic quantity of these micelle forming systems is the CMC. The volume fractions of both polymers $i=1,2$ in the bulk for the smallest micelles is exactly the same (by construction) and given by $\varphi_i^b(\text{CMC})$. Figure 6(a) presents the number of molecules per unit volume, which is given by

$$c^b = \frac{\varphi_1^b + \varphi_2^b}{N_B + 40}, \quad (28)$$

where we mention again that this number concentration is computed for the systems that have the smallest stable micelles possible (i.e., at the CMC). Inspection of the closed symbols in Fig. 6(a) (left ordinate), shows that the number concentration is a very weak function of the length of the

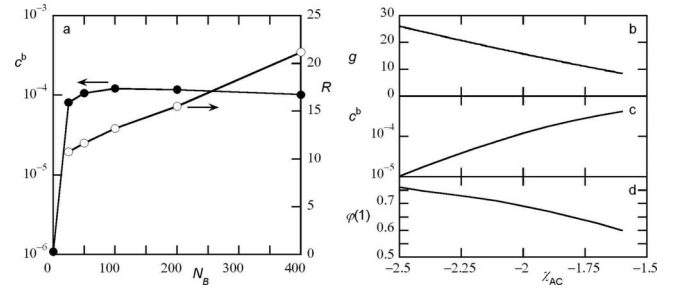


FIG. 6. (a) The number of polymer molecules per unit volume in the bulk c^b at the CMC (closed spheres, left ordinate) and the size of the corresponding micelles R (open points, right ordinate) as a function of the length of the corona block N_B . (b) The aggregation number g of micelles at the CMC as a function of the strength of the driving force χ_{AC} . (c) The corresponding number concentration $c^b(\chi_{AC})$, and (d) the corresponding volume fraction of the core forming block in the center of the micelle $\varphi(1)$. In (b)–(d) the value of $N_B=100$, in (a) $\chi_{AC} = -2$. Other parameters as in Fig. 5.

corona forming block. For comparison, a data point for $N_B = 0$ has been added to this figure. It corresponds to the number concentration of polymers in the system that has phase separated from a polymer-rich phase composed of A_{40} and C_{40} chains (see previous section). Apparently the number concentration of polymers that coexists with micelles is two orders of magnitude higher than expected from the phase diagram of the core forming blocks only. Note that the result of Fig. 6(a) implies that the polymer concentrations φ_i^b at the CMC increases almost linearly with N_B .

In the same figure, the micelle size R is presented, here defined as the first moment over the distribution of the corona block:

$$R = \frac{\sum_r L(r)r[\varphi_B(r) - \varphi_B^b]}{\sum_r L(r)[\varphi_B(r) - \varphi_B^b]}. \quad (29)$$

From Fig. 6(a), right ordinate, it is seen that the micelle size R increases linearly with the length of the corona block N_B , which is in excellent agreement with our recent experimental findings [19]. This linear dependence is typical for molecular brushes, i.e., it clearly indicates that the corona blocks are overlapping and stretched in the radial direction.

Figures 6(b)–6(d) show selected results for the dependence of the first stable micelles (i.e., micelles at the CMC) on the strength of the driving force χ_{AC} for the case that the copolymers have a corona forming block length $N_B=100$. With a decreasing strength of the driving force, i.e., χ_{AC} less negative, the aggregation number g decreases from close to $g=25$ for $\chi_{AC} = -2.5$ to $g \sim 10$ for $\chi_{AC} = -1.6$ [Fig. 6(a)]. The corresponding number concentration of polymers in the bulk, c^b , increases by more than a decade from close to $c^b = 10^{-5}$ to $c^b \sim 4 \times 10^{-4}$. The third property that is plotted in Fig. 6(d) is the polymer concentration in the center of the core, $\varphi(1) \equiv \varphi_A(1) + \varphi_C(1)$. As expected, this concentration drops with decreasing strength of the driving force. This implies that the volume fraction of water in the core, $\varphi_W(1) \approx 1 - \varphi(1)$, in-

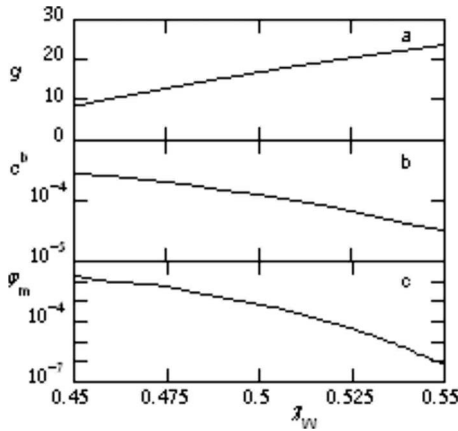


FIG. 7. (a) The aggregation number g of micelles at the CMC as a function of the “solvency” parameter χ . (b) The corresponding number concentration of polymers in the bulk, $c^b(\chi)$. (c) The corresponding volume fraction of micelles. In all cases $N_B=100$ and $\chi_{AC}=-2$. Other parameters as in Fig. 5.

increases with decreasing driving force. From Fig. 6(d) it is seen that the driving force must be rather low before the volume fraction of water in the core is larger than that of the polymer.

Above we have seen that the solvent quality χ strongly influences the associative phase behavior of A_{40} and C_{40} chains (Fig. 3). Hence, a similar strong influence of this parameter on the micelle formation of the block copolymers might be expected, namely, the better the solvent quality the lower the tendency of the core forming blocks to coassemble. This trend is illustrated in Fig. 7. Indeed with increasing solvent quality, i.e., lower χ , the smaller the aggregation number g at the CMC, the higher the bulk concentration above which micelles form [in Fig. 7(b) represented by the number concentration c^b], and the higher the concentration of micelles at the CMC. The latter quantity is computed from $\varphi_m = \exp(-(\varepsilon_m/k_B T))$, as the translational entropy of the micelle compensates the work of formation of the micelle [Eq. (6), correct only for dilute solutions where $\varphi_m \ll 1$]. One may wonder why stable micelles can form for $\chi > 0.5$. We propose to attribute this effect to the finite length of the corona forming block N_B , i.e., the block will not collapse in the poor solvent before $N_B(1-2\chi) \ll 1$. Furthermore, such micelles may show a tendency to aggregate, especially at a high micelle concentration (not accounted for). For example, the aggregation observed in aqueous solutions of CCCMs of P2MVP-*b*-PEO [poly(*N*-methyl-2-vinyl pyridinium iodide)-*block*-poly(ethylene oxide)] and PAA-*b*-PVOH [poly(acrylic acid)-*block*-poly(vinyl alcohol)] may be related to the fact that water is only a marginal solvent for PVOH [22]. Focusing on the lower values of χ , we see that the micelle concentration at the CMC becomes extremely high. This means that one will only see micelles in such systems if the overall polymer concentration is high and, moreover, one should also account for intermicellar interactions for such high concentrations of micelles.

In the above results we have taken $\chi \equiv \chi_W = \chi_B$ where $\chi_W \equiv \chi_{AW} = \chi_{BW} = \chi_{CW}$ and $\chi_B \equiv \chi_{AB} = \chi_{BC}$. In general, a repul-

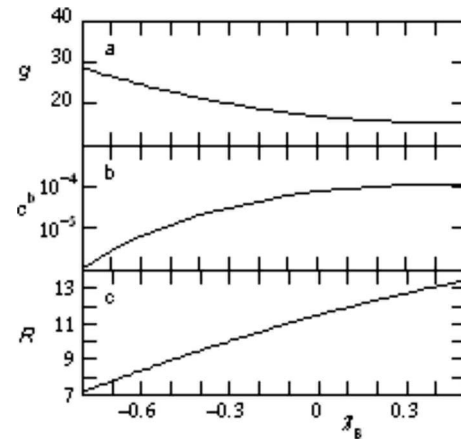


FIG. 8. (a) The aggregation number g of micelles at the CMC as a function of the interaction of the B segments with the other polymer segments χ_B . (b) The corresponding number concentration of polymers in the bulk, $c^b(\chi)$. (c) The corresponding size of the micelles, R . In all cases $N_B=100$, $\chi_{AC}=-2$, and $\chi_W=0.5$. Other parameters as in Fig. 5.

sion between core and corona forming segments (as used above) helps the formation of well-defined regions (core, corona) in a micelle. For classical ionic as well as nonionic micelles it has been found that such repulsion is needed to find good correspondence with experimental data. For the obligatory coassembly, a strong repulsion between core and corona forming blocks is not necessarily present. It is therefore of significant interest to investigate the effect of $\chi_W \neq \chi_B$. From the above it is reasonable to select the θ condition for the interactions of the polymer units with the solvent, i.e., $\chi_W=0.5$, and to vary the way the B units interact with the two other blocks. For this part of the investigation we select once again the system with $N_B=100$, and as $\chi_{AB}=\chi_{BC}$ was chosen, the system still qualifies as being symmetric.

In Fig. 8 we show that the interaction of the B segments with the other segments, i.e. with A and C has a strong influence on the micellar properties. Above a reasonable but not extremely strong repulsion of $\chi_B=0.5$ was used. Results in Fig. 8 show what happens when the repulsion is reduced and subsequently turned into an attraction. For the case of $N_B=100$, no stable micelles were found for very negative values of χ_B . We will return to this issue below. Figure 8(a) shows that the aggregation number has the tendency to increase when the repulsion between core and corona blocks is decreased. Indeed the repulsion between these units is part of a stopping force for micelle formation. When the stopping mechanism is weakened, an increase in the aggregation number should be expected. Interestingly, the size R of the micelle, which was measured by the first moment over the B segments, decreases [Fig. 8(c)]. This can be explained by a gradual overlap of B segments with the core segments, as will be presented below. The third quantity plotted in Fig. 8(b) is the number concentration of polymers in the bulk at the first appearance of micelles. The effect of χ_B on this quantity is very large. The attraction between the B and A or C segments strongly reduces c^b . The coassembly of A , C , and B can already occur at very low polymer concentrations.

The results of Fig. 8 are perhaps best rationalized by discussing a typical radial volume fraction profile of a stable

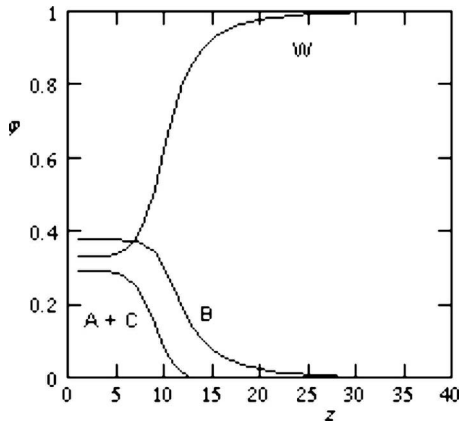


FIG. 9. Radial volume fraction profile for a micelle (at the CMC) formed by $A_{40}B_{200}$ and $C_{40}B_{200}$ copolymers with $\chi_B = -1.5$. Other parameters: $\chi_W = 0.5$, $\chi_{AC} = -2$.

micelle existing under a significant attraction between B and A or C segments. Figure 9 shows a micelle at the CMC for the case that $N_B = 200$ and $\chi_B = -1.5$. For such a long B block the micelles remain stable even at very negative χ_B values. The radial volume fraction profile of Fig. 9 must be compared to the ones shown in Fig. 5(a). There are several noteworthy differences. The most important difference is that the B block has a monotonically decreasing density profile, being highest in the center of the micelle and decreasing toward the periphery of the micelle until it is equal to the bulk concentration (found for $r > 25$). As the B block is much longer than the A or C block, there still is a coronalike layer outside the $(A-C)$ -rich core. Apparently, such a corona is still sufficient to restrict the aggregation of the copolymers to the colloidal domain. The second important issue is that the density of $A+C$ in the core is significantly lower in Fig. 9 as compared to Fig. 5(a). Simultaneously, the volume fraction of water in the core increased significantly. Indeed, from Fig. 9 it is easily understood why the measure of the micelle size R is so low: many of the B segments are now residing in the core. The third important difference is that the core is much larger in size for $\chi_B = -1.5$. This explains the relatively large aggregation number as reported in Fig. 8(a).

Radial volume fraction profiles of the type of Fig. 9 can lead to stable micelles only for copolymers with a B block much longer than the A or C blocks. Indeed, for short B blocks there is the risk that the “corona” block can be taken up by the core, depending on the strength of the attraction naturally. Indeed, for $\chi_B < -0.33$ no stable micelles were formed by copolymers with $N_B = 25$. Copolymers with a corona forming block $N_B = 50$ were stable as long as $\chi_B > -0.52$, where for $N_B = 100$ the critical interaction strength appeared close to $\chi_B = -0.8$. This observation may be relevant in experimental cases where attraction between corona and core forming segments can not be excluded. For example, under acidic conditions, poly(acrylic acid) PAA (core forming segment) is known to form H-bonded complexes with a large variety of neutral, water-soluble polymers, such as poly(ethylene oxide) PEO, poly(acrylamide) PAAM, poly(vinyl alcohol) PVOH, and poly(isopropyl acrylamide) PNIPAAm (corona forming segments) [23]. For CCCMs

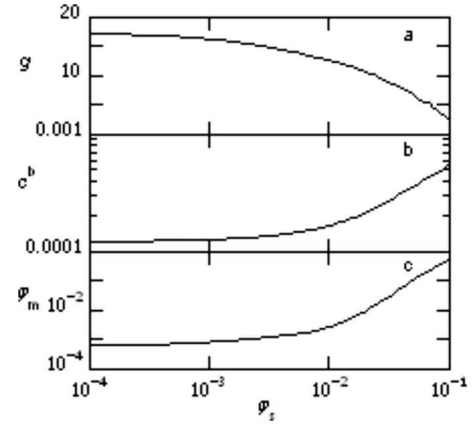


FIG. 10. (a) The aggregation number g of micelles at the CMC as a function of the volume fraction of “salt” ϕ_s (on logarithmic scale), (b) the corresponding number concentration of polymers in the bulk, $c^b(\phi_s)$, and (c) the corresponding volume fraction of micelles ϕ_m . In all cases $N_B = 100$, $\chi_{AC} = -2$, and $\chi = 0.5$. Other parameters as in Fig. 5.

of PAA-*b*-PNIPAAm and P2MVP-*b*-PEO, precipitation was observed under acidic conditions where PAA forms insoluble complexes with both PEO and PNIPAAm, i.e., attraction between core and corona forming segments was found to destabilize the CCCMs [24].

Micelle formation in the presence of “salt”

The results on the associative bulk phase behavior of A_{40} and C_{40} in a common solvent showed that the driving force for the formation of a coacervate phase is reduced in the presence of a pair of monomeric components P and N , where a P monomer is equivalent to an A segment and a N monomer to a C segment. Indeed the presence of the “salt” screens the attractive interactions between A and C , similarly to the true effect of salt when the associative driving forces are due to the attraction between positively and negatively charged units. A similar effect is expected for the formation and stability of CCCMs. In Fig. 10, we present how a selection of micellar properties is affected by a background concentration of salt, where ϕ_s corresponds to the concentration of the monomeric species in the water rich bulk phase. Again, the concentration of P and N monomers in the bulk was kept equal at $\phi_s \equiv \phi_P = \phi_N$ (the subscript s refers to the notion of a salt).

Basically, the addition of salt has the same effect as a reduction of the driving force for self-assembly. Therefore, the results of Fig. 10 must be compared with those presented in Figs. 6(b)–6(d). Even though the N monomers like to interact with the A segments and the P monomers have an affinity for the C segments, the salt components are depleted from the core. As long as the concentration of the salt ions in the bulk remains low, the number of small ions in the core remains even lower and the micellization is basically unaffected by the presence of salt. As a result, the aggregation number g (at the CMC), the number volume fraction of polymer in the bulk, c^b , and the micelle concentration (at the CMC) ϕ_m are essentially independent of ϕ_s as long as ϕ_s

$< 10^{-2}$. Then, upon further increase of the ionic strength (in the bulk), gradually also the salt concentration in the core of the micelle increases, reducing the number of A-C contacts. As a result the aggregation number decreases [Fig. 10(a)], the number concentration of polymers in the bulk increases [Fig. 10(b)], and the micelle concentration at the CMC increases strongly (ε_m decreases). As discussed above, the latter effect implies that, even though the aggregation number decreases (to very low values) the total polymer concentration needed to find micelles becomes very high at high ionic strengths. Experiments for which the overall polymer concentration is fixed will witness a disappearance of micelles above some threshold ionic strength. Both effects are indeed observed in experiments [1,4,5,25].

Figure 6(b) illustrated that for a system with a smaller intrinsic driving force, i.e., not so negative χ_{AC} , the threshold ionic strength below which a coacervate phase is stable is lower. Similarly, we must expect that micelles become less stable against dissolution by salt, when the driving force for assembly is reduced, and vice versa. In the same token we must anticipate that the amount of salt needed to prevent micellization is a function of the solvent quality χ_w , as well as a strong function of the segment-segment interaction parameter χ_B .

Asymmetric ternary systems

Up to this point we have focused on symmetric systems. The reason for this choice is clear, as any type of asymmetry significantly increases the level of complexity, hampering a proper analysis of the SCF results. Only for the symmetric case can one expect the bulk concentrations of the two associating molecules to remain equal to each other and the volume available per micelle, a quantity that is not known *a priori*, can be dealt with straightforwardly. As soon as the bulk concentrations are not equal, however, there is an unequal partitioning of the two molecular components between the bulk and the micelle. As a consequence, the volume available per micelle must be known to evaluate the composition in the system: a change in the volume available per micelle automatically leads to a change in the ratio between the number of molecules of types 1 and 2 in the system. Of the many asymmetric cases that one can construct, we select the case of the formation of micelles composed of copolymers $i=1$, $A_{40}B_{100}$, mixed with homopolymers $i=2$, C_{40} in a nonselective solvent as represented by the equilibrium



We may expect that the micelles composed of this set of molecules have aggregation numbers such that $g_1 \approx g_2$. However, in general there is a difference between g_1 and g_2 simply because the C_{40} molecule will have a higher tendency to be part of a micelle than the copolymer $A_{40}B_{100}$. Nevertheless, there may be bulk concentrations φ_1^b and φ_2^b for which the micellar stoichiometry is exactly maintained. The problem is how to find this composition. We may further anticipate that micelles composed of a copolymer and a homopolymer can form easier than with two copolymers, because the homopolymer is not accompanied by a corona block. There are also significant consequences for the overall

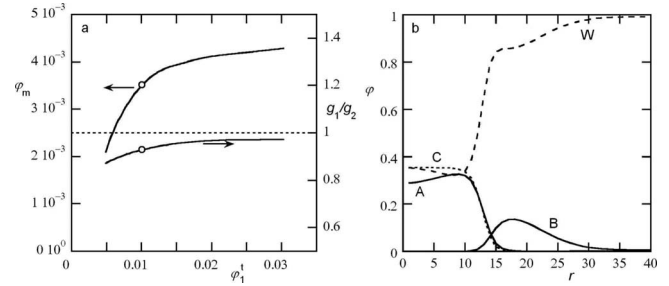


FIG. 11. (a) The volume fraction of micelles φ_m (left ordinate) and the ratio between the number of copolymers $A_{40}B_{100}$ and homopolymers C_{40} in the micelle, g_1/g_2 (right ordinate) as a function of the overall volume fraction of copolymer in the system for a given total volume fraction of homopolymer $\varphi_2^t=0.001$. The open spheres point to the system presented in (b). (b) The radial volume fraction profiles of the components in the system for the micelle pointed at by the open spheres in (a). Parameters: $\chi_{AB}=-2$, $\chi=0.5$.

aggregation numbers, etc. Experimentally accessible is the overall concentration of the two polymers in the system. The overall volume fraction of molecule $i=1$, φ_1^t , can be estimated from the SCF calculations from the mass balance equation

$$\varphi_1^t = \varphi_1^b + f_1 \varphi_m = \varphi_1^b + \frac{g_1 N_1}{g_1 N_1 + g_2 N_2} \exp - \frac{\varepsilon_m}{k_B T}, \quad (31)$$

where f_1 is the fraction (based on the volume) occupied by the copolymer ($i=1$) in the micelle. A corresponding equation is available for the total volume fraction of the homopolymer ($i=2$). In Fig. 11, the total volume fraction of the homopolymer was fixed to $\varphi_2^t=0.001$ and the overall volume fraction of the copolymer φ_1^t was varied. Note that the number concentrations of the two components are found after division by the chain length $N_1=140$ and $N_2=40$, respectively.

Figure 11(a) shows that the overall composition in the micelles (corresponding to the ratio g_1/g_2) remains close to unity for all micelles, upon an increase of the copolymer concentration by as much as a decade. Upon closer inspection, however, we observe that the ratio remains slightly below unity, indicating that the copolymer is slightly underpopulated in the micelle. Obviously, this disparity from stoichiometry decreases with increasing copolymer concentration. If one decreases φ_2^t or increases φ_1^t , it is possible to obtain micelles that are overpopulated by copolymers (data not shown). Furthermore, Fig. 11(a) shows that the overall volume fraction of micelles increases with increasing copolymer concentration. As in first order the micellization is given by reaction (30), such a result is natural and must be expected. The more copolymers are added, the more homopolymers are consumed to form micelles. However, in static light scattering (SLS) experiments studying CCCM formation, one typically finds a maximum in the SLS intensity at a certain mixing fraction upon gradual addition of the homopolymer (e.g., C_{40}) to a solution of copolymers (e.g., $A_{40}B_{100}$), i.e., at both very low and very high copolymer concentration, the SLS intensity is low [4,22,26,27]. At this

mixing fraction, denoted as the preferred micellar composition (PMC), the CCCMs are argued to be of stoichiometric composition, the most favorable, and the largest in mass and/or number. The “classical” interpretation to rationalize this maximum in the SLS intensity is to postulate the existence of soluble complexes with some excess charge (i.e., overpopulated by either copolymers or homopolymers) on either side of the PMC for mixing fractions that deviate from the PMC [20]. As discussed above, such soluble complexes are not accounted for in the present model, and as a consequence, the experimentally observed maximum in micellar number and/or mass is not reproduced.

As an example, in Fig. 11(b) we present radial volume fraction profiles for the copolymer (solid line, φ_A and φ_B), the homopolymer (dotted line, φ_C), and the solvent (dashed line, φ_W) for the system with $\varphi_1^f=0.01$. In this case the grand potential is $\varepsilon_m=5.65k_B T$, i.e., close to the micelles presented in the previous section. The overall profiles can thus be compared to those given in Fig. 5(a). Note that in Fig. 11(b) the A and C profiles are plotted separately and not added together as in Fig. 5(a). In this example, $g_1 \approx 66$ and $g_2 \approx 71$. These aggregation numbers are significantly larger than for the micelles composed of a pair of copolymers (as also found experimentally [4,26]). This increase in the aggregation number has significant consequences for the radial volume fraction profiles. The core is much thicker, the corona extends to larger distances ($R=20.1$), and the maximum density in the corona is much higher. The number concentration of the copolymer $c_1^b=5.5 \times 10^{-5}$ is very close to that found above. The homopolymer number concentration is $c_2^b \approx 4 \times 10^{-6}$, which is a factor of ten lower than that of the copolymer. Such an asymmetry in the bulk concentration has already been discussed for the phase diagrams of homopolymers (Fig. 2).

Close inspection of Fig. 11(b) shows that the homopolymer C is distributed homogeneously through the core. The copolymer, however, has an inhomogeneous distribution. The density of the A block decreases toward the center. As a result, the mismatch between the local concentrations $\varphi_A(r) - \varphi_C(r)$ is highest in the center and lowest near the core-corona interface. The radial dependence of the mismatch of these densities is easily explained by realizing that the copolymer is effectively confined to be at the core-corona interface with the A - B link. The A block can not assume a random conformation, but instead, it needs to assume a rather stretched conformation. As the homopolymer does not have positional constraints, it can distribute more evenly. As the contribution of the stretching of the core blocks of the

copolymers to the stopping mechanism is less pronounced in the asymmetric case (as there are simply less copolymers present), it is compensated by a higher corona density. In other words, a larger fraction of the stopping force for micellar growth must stem from the crowding of B chains in the corona, i.e., the pressure in the corona must be higher, so that the density in the corona become much higher.

CONCLUSIONS

Without explicitly taking into account the fact that the coassembly is driven by charge-charge interactions, we have presented a thermodynamically consistent SCF analysis for obligatory coassembly of (co)polymers leading to spherical micelles. In this primitive model, the attractive interactions are treated on the Flory-Huggins short-range interaction level. It was shown that one can learn much about obligatory coassembly from this model. The results are expected to be qualitatively correct, as many of the predictions were shown to be in qualitative agreement with experimental findings on CCCMs, and may be applied to systems where coassembly is driven by other mechanisms, such as H bonding. Even in this primitive model, only the symmetric systems are easily analyzed. Symmetric systems have the property that the two components necessary for coassembly have the same bulk concentrations, the same contribution to the overall aggregation number, etcetera. Any deviation from this academic case (which may arise from a difference in molecular composition of the two components, from differences with respect to the solvent quality, and/or from differences in the concentration composition), significantly complicates the analysis. Still, in principle, such asymmetric systems can be analyzed and experimentally relevant predictions can be made. We anticipate that future theoretical work on electrostatically driven obligatory coassembly, will focus on bulk correlations leading to the experimentally observed soluble complexes and how to take the electrostatic nature of the driving force into account explicitly.

ACKNOWLEDGMENTS

This work is part of the research programme of the Stichting voor Fundamenteel Onderzoek der Materie (FOM), which is financially supported by the Nederlandse Organisatie voor Wetenschappelijk Onderzoek (NWO). It has been carried out in the framework of the EU Polyamphi/Marie Curie program (FP6-2002, Proposal No. 505027). I.V. was financed by the SONS Eurocores program (Project No. JA016-SONS-AMPHI).

[1] A. V. Kabanov, T. K. Bronich, V. A. Kabanov, K. Yu, and A. Eisenberg, *Macromolecules* **29**, 6797 (1996).
 [2] A. Harada and K. Kataoka, *Macromolecules* **28**, 5294 (1995).
 [3] M. A. Cohen Stuart, N. A. M. Besseling, and R. G. Fokkink, *Langmuir* **14**, 6846 (1998).

[4] I. K. Voets, A. de Keizer, and M. A. Cohen Stuart, *Adv. Colloid Interface Sci.* (to be published), doi: 10.1016/j.cis.2008.09.012
 [5] M. A. Cohen Stuart, B. Hofs, I. K. Voets, and A. de Keizer, *Curr. Opin. Colloid Interface Sci.* **10**, 30 (2005).
 [6] M. Castelnovo, *Europhys. Lett.* **62**, 841 (2003).

- [7] E. Y. Kramarenko, A. R. Khokhlov, and P. Reineker, *J. Chem. Phys.* **125**, 194902 (2006).
- [8] E. Y. Kramarenko and A. R. Khokhlov, *Polym. Sci., Ser. A Ser. B* **49**, 1053 (2007).
- [9] J. Lee, Y. O. Popov, and G. H. Fredrickson, *J. Chem. Phys.* **128**, 224908 (2008).
- [10] D. G. Hall and B. A. Pethica, in *Nonionic Surfactants*, edited by M. Schick (Marcel Dekker, New York, 1967), Vol. 1, pp. 516–567.
- [11] T. L. Hill, *Thermodynamics of Small Systems* (W.A. Benjamin, New York, 1963/Dover, Mineola, NY, 1994), Vol. 1.
- [12] T. L. Hill, *Thermodynamics of Small Systems* (W.A. Benjamin, New York, 1964/Dover, Mineola, NY, 1994), Vol. II.
- [13] F. A. M. Leermakers and J. Scheutjens, *J. Phys. Chem.* **93**, 7417 (1989).
- [14] F. A. M. Leermakers and J. Scheutjens, *J. Colloid Interface Sci.* **136**, 231 (1990).
- [15] F. A. M. Leermakers, C. M. Wijmans, and G. J. Fleer, *Macromolecules* **28**, 3434 (1995).
- [16] Y. J. Li, P. L. Dubin, H. A. Havel, S. L. Edwards, and H. Dautzenberg, *Langmuir* **11**, 2486 (1995).
- [17] H. G. Bungenberg de Jong, in *Colloid Science*, edited by H. R. Kruyt (Elsevier, Amsterdam, 1949), Vol. II, Chap. X.
- [18] A. A. Freitas, F. H. Quina, and F. A. Carroll, *J. Phys. Chem. B* **101**, 7488 (1997).
- [19] I. K. Voets, S. van der Burgh, B. Farago, R. Fokkink, D. Kovacevic, T. Hellweg, A. de Keizer, and M. A. Cohen Stuart, *Macromolecules* **40**, 8476 (2007).
- [20] S. van der Burgh, A. de Keizer, and M. A. Cohen Stuart, *Langmuir* **20**, 1073 (2004).
- [21] E. B. Zhulina and O. V. Borisov, *Macromolecules* **38**, 6726 (2005).
- [22] I. K. Voets, A. Debuigne, C. Detrembleur, R. Jérôme, A. de Keizer, and M. A. Cohen Stuart (unpublished).
- [23] V. V. Khutoryanskiy, G. A. Mun, Z. S. Nurkeeva, and A. V. Dubolazov, *Polym. Int.* **53**, 1382 (2004).
- [24] I. K. Voets, P. M. Moll, A. Abdelhafid, C. Jérôme, C. Detrembleur, P. de Waard, A. de Keizer, and M. A. Cohen Stuart, *J. Phys. Chem. B* **112**, 10833 (2008).
- [25] Y. Yan, N. A. M. Besseling, A. de Keizer, M. Drechsler, and M. A. Cohen Stuart, *J. Phys. Chem. B* **112**, 10908 (2008).
- [26] B. Hofs, I. K. Voets, A. de Keizer, and M. A. Cohen Stuart, *Phys. Chem. Chem. Phys.* **8**, 4242 (2006).
- [27] I. K. Voets, C. Weise, S. M. King, A. de Keizer, U. Scheler, and M. A. Cohen Stuart (unpublished).